

## Investigation of photocatalytic degradation of an anionic dye Brilliant Blue G 250 by nanocatalyst of ZnO-EG prepared under ultrasonic waves

Ikram Boukerche<sup>a,b,\*</sup>, Zineb Boutamine<sup>b</sup>, Sara Bekrou<sup>c</sup>

<sup>a</sup>Normal High School of Technological Education (ENSET), email: s\_ikram06@yahoo.fr

<sup>b</sup>Laboratory of Process Engineering for Sustainable Development and Health Products, Department of Process Engineering, National Polytechnic School of Constantine, BP 75, A, Nouvelle Ville RP, Constantine, Algeria, email: boutaminezineb@gmail.com

<sup>c</sup>Laboratory of Environmental Engineering, Department of Process Engineering, Badji Mokhtar – Annaba University, P.O. Box 12, 23000 Annaba, Algeria, email: sarabekrou@yahoo.com

Received 3 February 2022; Accepted 16 December 2022

### ABSTRACT

Semiconducting metal oxides have been proven to be good candidates as sensitive materials for photocatalysts in the removal reactions of polluting molecules. This study presents a simple procedure for producing zinc oxide “ZnO” with a diameter of fewer than one hundred nanometers using an aqueous solution of zinc sulfate heptahydrate ( $ZnSO_4 \cdot 7H_2O$ ) and sodium hydroxide under ultrasonic waves in the presence of ethane-1,2-diol (EG), polyethylene glycol (PEG400, PEG4000) as dispersing media. The influence of concentration and the nature of the surfactant agent were discussed in detail. The resulting powder is calcined at temperatures between 500 and 1,000°C for 4 h. The solids are characterized using X-ray diffraction (XRD), scanning electron microscopy, energy-dispersive X-ray analysis, and Fourier-transform infrared spectrometry. The XRD pattern reveals that the nanoparticles are in a well-crystalline phase. The particle size estimated from dynamic light scattering confirms the small size of the studied ZnO-NPs. The average diameters range from 16.45 to 35.19 nm with EG and PEG400 at 0.01 M, respectively. The Brunauer–Emmett–Teller surface area of the synthesized ZnO-NPs is about 134.831 m<sup>2</sup>/g. Photocatalytic degradation of Brilliant Blue G 250 in an aqueous solution was performed using the ZnO-EG as a photocatalyst. The results showed that the efficiency of 87.43% is reached after 60 min of treatment for a mass/liquid ratio equal to 0.5 at natural pH. The efficiency increases with the increase in the mass of the ZnO-EG to reach 94.32% for the optimal ratio equal to 1. The increase in the dye concentration decreases the effectiveness of the treatment. The degradation is better in alkaline conditions.

*Keywords:* Zinc oxide; Nanoparticles; Photocatalyst; Surfactant agent; Brilliant Blue dye

### 1. Introduction

Water is the main resource of all socio-economic sectors. Unfortunately, with the rapid development of industrialization, it has been deteriorating, sometimes irreparably [1]. The textile industry is one of the most water-intensive industries and uses organic dyes to color its products [2]. The problem is that these dyes, highly charged with toxic compounds, are released into the environment, creating

a serious problem for many countries [3]. Effluents from dye manufacturing plants and the industries that consume them are highly colored and characterized by high pH variations, high biochemical oxygen demand, and increased biotoxicity to bacteria [4].

Dyes reduce sunlight penetration into receiving waters, delay photosynthesis, and over-suppress the growth of aquatic flora [5]. Dyes can also harm waters when they undergo anaerobic degradation in sediments due to the

\* Corresponding author.

formation of highly toxic amines resulting from their incomplete degradation by bacteria [6]. They can also cause dermatitis and even skin cancer in humans. Most of these contaminants escape conventional wastewater treatment [7]. These emerging environmental pollutants are a concern for environmental agencies [8]. To limit the arrival of these different types of refractory contaminants in the environment, efficient and environmentally friendly treatment strategies have been developed. Advanced oxidation processes (AOPs) are the first among these strategies [5].

AOPs rely on the *in-situ* generation of highly oxidizing radicals, primarily hydroxyl radicals ( $\text{HO}^\bullet$ ). Hydroxyl radicals can oxidize many organic compounds with a higher oxidation rate than ozone (109 times higher) [9]. Free radicals are highly active species that can react with almost any organic molecule [10]. These AOPs have been applied in several sectors to treat the surface, groundwater, and environmental protection. Photocatalysis in the presence of semiconductors is among the cheapest and most promising AOPs [11]. It has become a rapidly growing field of research over the past decades [12]. This technique is widely used in wastewater treatment due to its low cost, non-toxicity, and efficient performance in the total mineralization of organic pollutants [13]. This technique is based on the excitation of a semiconductor by a light source (UV or visible) [14]. The wavelength of this light radiation must be less than 400 nm corresponding to an energy  $h\nu$  equal to or greater than the bandgap ( $E_g$ ) to create strongly oxidizing reactive species that will lead to the photodegradation of organic pollutants [15].

In the context of this work, we chose an anionic dye, the Brilliant Blue G 250, also called Coomassie Blue, widely used on the African Continent, especially in the textile industry [16]. It is considered an integral component of the Bradford method for determining proteins in solution [17]. The paper describes the growth parameters to obtain ZnO nanostructures using the ultrasound-assisted technique [18]. Zinc oxide is abundant and non-toxic on earth and is low-cost, unlike other materials like  $\text{TiO}_2$  [19–22]. ZnO is a chemical compound with the formula ZnO. It is insoluble in water but soluble in acids and alcohols. It is highly sought after because of its interesting properties, and its many advantages make it a material that rivals other oxides on the market [23,24].

There are three types of crystallographic structures of ZnO, depending on the conditions of elaboration: the hexagonal structure, which is stable under normal conditions. The cubic structure, which is unstable and appears under high pressure, and the rock-salt structure. ZnO crystallizes according to the most stable structure at room temperature, that is, the wurtzite structure, in which the oxygen ions are arranged in a compact hexagonal lattice and/or the zinc atoms occupy half of the tetrahedral interstitial positions having the same arrangement as the oxygen ions, ZnO is a wide direct gap semiconductor at  $E_g$  3.3 eV at 385 nm at room temperature, it has the highest piezoelectric effect of all semiconductors (relative dielectric constant equal to 8.75 this effect is closely related to its crystal structure, its refractive index has a value that varies between 1.90 and 2.20 [25,26], it has the highest exciton binding energy of the semiconductors of 60 meV, in general ZnO is non-toxic and

biocompatible, relatively simple to synthesize at low cost, it is physically and chemically stable, it also has a good sensitivity to variations in environmental conditions to which it is subjected. These different properties make it a semiconductor of choice in various applications, such as photovoltaic cells, light-emitting diodes, surface electrodes, energy generators or recuperators, gas sensors, and photocatalytic reactors for air and water purification. In addition, to all these advantages, in the photocatalytic degradation of different dyes, ZnO exhibited better photocatalytic efficiency than  $\text{TiO}_2$ , although the band gap energy of ZnO is the same as that of  $\text{TiO}_2$  (~3.2 eV) [27–29].

The main objective of this work is the elaboration and study of the photocatalytic properties of ZnO nanostructures, starting from the decrease of the grain size up to the nanometric scale, presents new physicochemical properties and opens promising perspectives in terms of applications in environmental chemistry [30]. The ultrasonically assisted route is an interesting method that has become increasingly popular for synthesizing metal oxide nanoparticles [31]. The advantages of this technique over other methods include the fact that the reaction rate is fast, the reaction conditions are controllable with the ability to form nanoparticles with uniform shapes, and it ensures narrow size distributions and high purities. It has been widely used to generate new materials with unusual properties since, in many cases, it causes the formation of particles of much smaller size and higher surface area than those reported by other methods [32].

A crucial factor for the formation of nanoparticles under ultrasonic irradiation is the selection of the solvent. Since the type of solvent considerably affects the size and shape of the nano-product obtained, generally, water is one of the best solvents due to its high dipole moment. Nevertheless, ethylene glycol (EG) is considered more suitable. It has a higher dipole moment and acts as a solvent and a reducing and stabilizing agent to control growth and prevent agglomeration [33]. On the other hand, polyethylene glycol (PEG) is a suitable surfactant to stabilize nanoparticle dispersions to improve the surface. In addition, PEG solutions are less toxic, biodegradable and environmentally friendly [34,35].

This paper mainly focuses on improving the properties of zinc oxide by seeking the best synthesis conditions and designing a process to control the morphology and size of the latter to increase its catalytic capabilities to achieve a better yield in the photocatalytic process in the removal of textile dyes. The fact that the dyes are not easily biodegradable in aerobic conditions due to the complexity of their chemical structure and the presence of aromatic rings implies that the corresponding aqueous effluents require a specific treatment due to the singular impact that they cause in the natural environments (toxicity of the parent product and possible by-products) [36,37]. Conventional treatments (adsorption on activated carbon, membrane processes, coagulation–flocculation, chemical oxidations) have the disadvantage of transferring the pollution from an aqueous phase to a new phase, and lead for the most part to the formation of concentrated sludge, creating a problem of secondary waste or regeneration of materials often very expensive [38,39].

Furthermore, this study aims to investigate the photocatalytic performances of the synthesized “ZnO” photocatalyst during the removal of Brilliant Blue G 250 in an aqueous medium, as well as the study of the effects of the various operating parameters such as the initial concentration of the dye, the initial pH of the solution and the influence of the mass of our semiconductor on the effectiveness of the studied process. In this study, we chose zinc oxide as the photocatalyst to remove our model dye because it exhibits better photocatalytic activity than  $\text{TiO}_2$ , according to several previous works [40].

## 2. Experimental setup

### 2.1. Reagents and solutions

All the purchased reagents were used without further purification. An analytical-grade zinc sulfate heptahydrate  $\text{ZnSO}_4 \cdot 7\text{H}_2\text{O}$  (98%, Sigma-Aldrich, Germany) and sodium hydroxide NaOH (97%, Biochem Chemopharma, France) was used as the starting materials. They were dissolved in deionized water. Under continuous magnetic stirring, an aqueous solution of 0.5 mol/L  $\text{ZnSO}_4 \cdot 7\text{H}_2\text{O}$  was mixed with an appropriate amount of 5 and 10 mol/L NaOH solutions. The final pH of the mixed solutions was highly basic, with a pH of 14. To better control the growth of the particles that were formed, we also used PEG4000 (Sigma-Aldrich, Germany), PEG400 (Sigma-Aldrich, Germany), and EG (Honeywell, United States) as a capping agent to reduce particle agglomeration. Brilliant Blue G 250 with molecular formula  $\text{C}_{47}\text{H}_{48}\text{N}_3\text{NaO}_7\text{S}_2$  (Sigma-Aldrich 99%, Germany) was used as a molecule test for dye degradation.

### 2.2. Reactor

We performed the sono-synthesis of ZnO nanoparticles (NPs) using a continuous flow ultrasonic reactor (Fig. 1). The ultrasonic reactor consists of a 100 mL cell surrounded by a cylindrical jacket glass, which allows the reactor to be

cooled with water to control the temperature. The ultrasonic horn was immersed in the reactor from the top of the reactor. The ultrasonic irradiation was conducted with a programmable and microprocessor-based sonic processor Vibra-Cell (Sonics & Materials, Model: VCX 750). The ultrasonic probe of the processor was fabricated from high-grade titanium alloy and had a tip diameter of 25 mm. The ultrasound frequency generated by this probe was 20 kHz with a maximum power output of 750 W.

### 2.3. Synthesis of ZnO-NPs

According to our protocol, the synthesis of ZnO nanostructures depends on the nature of the polyol and its dosage. Several types of polyols were used, such as (PEG4000, PEG400 and EG). Due to its good solubility in these polyols, the metal precursor used in the whole study is zinc sulfate heptahydrate with the chemical formula  $\text{ZnSO}_4 \cdot 7\text{H}_2\text{O}$ . Sodium hydroxide (NaOH) was added to adjust the basicity of the medium. During the protocol, the precursor, polyol, water, and optionally base mixture was heated under reflux and stirred to a temperature between 120°C and 227°C maintained over a step of about 1 h. Initially, the progressive dissolution of the precursor in the polyol leads to a transparent solution. After 30 min of the experiment, a milky white precipitate appears visible to the naked eye.

The mixture is then cooled to room temperature. The precipitate corresponding to the oxide phase is recovered by centrifugation, washed with absolute ethanol, then with acetone, and vigorously dispersed in the ultrasonic reactor described above. Indeed, the acoustic bubbles produced by the sound wave offer an excellent facility similar to micro-reactors [41,42] with extremely severe operating conditions, resulting in a very high temperature and pressure estimated, respectively at 5.000 K and 1.000 atm [43,44], as well as an energy that can reach up to 13 V, these conditions give rise to the birth of extraordinary chemical reactions and create an environment favorable to the nucleation and growth of materials [45].

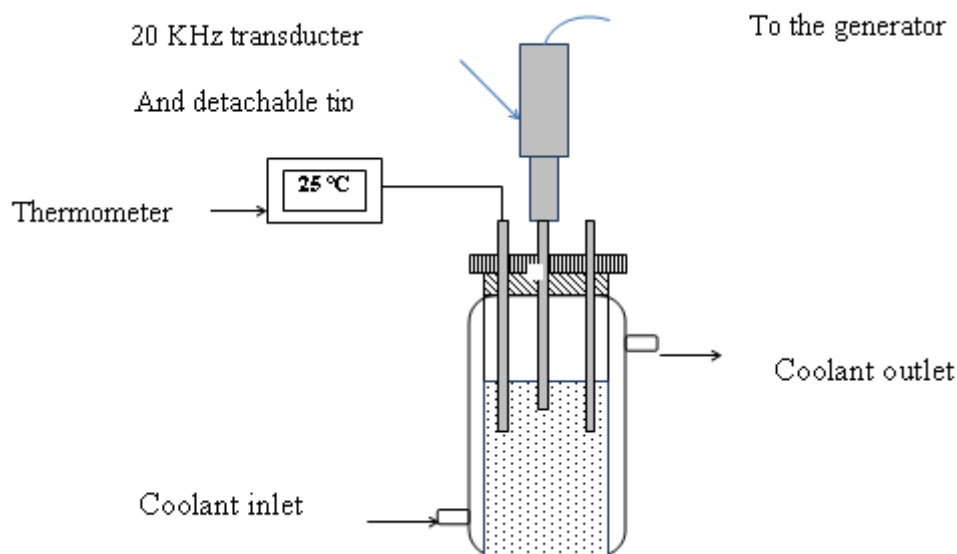


Fig. 1. Scheme of the continuous flow ultrasonic reactor.

The samples are centrifuged again. The ethanol and acetone washes are repeated several times until the supernatant becomes completely clear. The powder is then dried in an oven at 50°C. The resulting powder is calcined at temperatures between 500 and 1,000°C for 4 h to remove the surfactant residues and obtain a high-purity phase of the zinc oxide NPs. The temperature is also necessary for the crystallization of the formed powder. X-ray diffraction (Philips X'Pert Type Apparatus), scanning electron microscopy (SEM), Fourier-transform infrared (FTIR) spectroscopy (SHIMADZU IRAffinity-1S Type Apparatus), and Raman spectroscopy are used to study the structural and optical properties of the synthesized solids. The size of the formed particles was analyzed using a "Horiba SZ-100" nanosizer; the latter depends on dynamic light scattering (DLS, also known as photonic correlation spectroscopy or quasi-elastic light scattering) is one of the most popular light scattering techniques as it allows to size particles up to 1 nm in diameter. The basic principle is simple: the sample is illuminated by a laser beam, and fluctuations in the scattered light are detected at a known scattering angle  $\theta$  by a fast photon detector [46]. To confirm the results presented in this study, we repeated all the experiments at least three times to verify and validate our results. Table 1 summarizes the equipment used for analysis and synthesis.

#### 2.4. Photocatalytic degradation of Brilliant Blue G 250

The Brilliant Blue G 250 degradation experiments are performed in a cylindrical reactor with a 300-volume mL made of glass surrounded by an aluminum foil before the lamp is turned on to protect from the emitted UV radiation on the one hand and to avoid any reaction involving sunlight on the other hand. The lamp is placed in a quartz sheath transparent to the radiation and is immersed in an axial position centered in the reactor. The volume of water to be treated is 100 mL (Fig. 2).

The UV irradiation source is a UV lamp (254 nm, 1,100  $\mu\text{W}/\text{cm}^2$ ). Samples for solution analysis were collected by pipetting an aliquot of solution at well-defined time intervals. The effectiveness of the proposed procedure was evaluated by monitoring the degradation of Coomassie Blue G 250 (Brilliant Blue G 250) and measuring the absorbance at 587 nm. Measurement of species concentration during

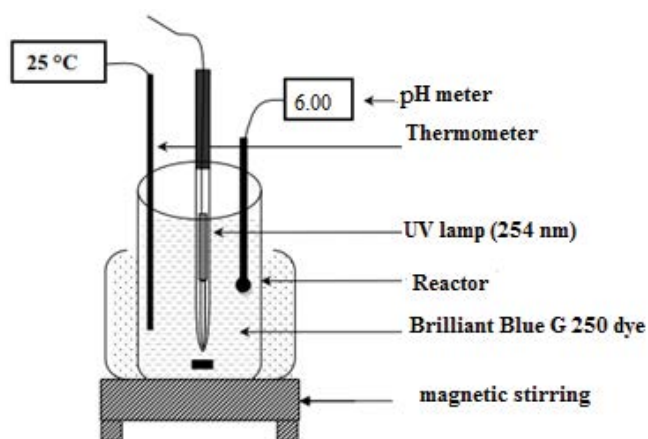


Fig. 2. Scheme of photocatalytic degradation reactor.

photolysis was performed using a UV-Visible spectrophotometer. To validate the results obtained, all the experiments were repeated several times.

### 3. Results and discussion

#### 3.1. Effect of nature and concentration of polyol on the growth mechanism

A series of syntheses were performed using EG, PEG400, and PEG4000 at different concentrations ranging from 0.01 to 0.5 M to investigate the influence of the nature and concentration of polyols on the growth mechanism and size of the formed ZnO nanoparticles. Table 2 and Fig. 3 list the obtained results. Like the sol-gel methods [47], the polyol process is a soft chemistry route that can control the nucleation and particle growth process by adding a polyol [48]. The interest of their use lies in their polar character and high boiling point, which allows them to solubilize a large number of metal precursors and activate the reactions [49].

Polyols are also reducing agents [50]. They are also suitable nucleation and growth media for particles in a finely divided state. They also act as surfactants that adsorb on the surface of elementary particles and avoid their agglomeration by steric hindrance [51]. Previous studies have shown that the mechanisms involved in the precipitation of oxides in polyol media are similar to hydrolysis and condensation reactions, governed by the amount of  $\text{OH}^-$  ion in the medium [52]. Within this framework, this study aimed to identify the role of  $\text{OH}^-$  ion concentration on the morphology and size of ZnO particles by varying the concentration of the different polyols. All tests in this series of experiments were performed by setting the concentration of zinc sulfate heptahydrate to 0.5 M and sodium hydroxide to 1 M. Table 2 summarizes the other parameters. It is important to note that the temperature of the medium is imposed by the boiling temperature of the polyols used.

The particles obtained in these experiments were first characterized by scanning electron microscopy (SEM) to determine their morphology. Fig. 7 indicates the results obtained. On the other hand, the size of the powder formed is estimated by dynamic light scattering. Based on the results, it can be noted that the smallest size was obtained with the lowest concentrations of polyols used. We detected particles of 16.45 nm with EG at 0.01 M against 454.52 nm with the same surfactant at 0.5 M.

The same observation was noted for the other polyols under the same operating conditions. Therefore, it can be said that as the concentration of polyol increases, the particle size increases. The effect of the length of the alkyl chain is studied by varying the nature of the polyol used (EG, PEG400, PEG4000). The average size of the particles obtained for all the powders synthesized increases according to the number of carbon atoms of the alkyl chain. Indeed, we obtained particles of 16.45, 35.19, and 191.13 nm with EG, PEG400, and PEG4000, respectively.

#### 3.2. Morphology and structure

Fig. 4 shows the UV-Visible absorption spectrum of the synthesized ZnO nanoparticles. The UV-Vis spectrum shows a characteristic absorption edge located at about

Table 1  
Equipment used

Equipment	Brand	Conditions	Country
BET	Quantachrome® ASiQwin™ – Automated Gas Sorption Data Acquisition and Reduction © 1994–2017, Quantachrome Instruments Version 5.21	Sample weight: 0.082 g; Instrument: Autosorb iQ Station 3; Approx. outgas; Time: 8.6 h; Final outgas temp.: 200°C extended info: available; Analysis gas: nitrogen; Non-ideality: 6.58e-05 1/Torr CellType: 9 mm; Analysis time: 8:23 h:min; Bath temp.: 77.35 K.	Austria
FTIR	IRAffinity-1S (SHIMADZU)	Interferometer Michelson interferometer (30° incident angle); Equipped with a dynamic alignment system; Sealed interferometer with auto dryer; Wavenumber range from 7,800 to 350 cm <sup>-1</sup> ; Resolution 0.5, 1, 2, 4, 8, and 16 cm <sup>-1</sup> ; S/N ratio 30,000:130,000:1, accumulation of 1 min, quarter of 2100 cm <sup>-1</sup> , automatic peak detection. Dynamic light scattering (DLS) technique; Measurement range; Particle diameter: 0.3 nm–8.0 μm;	Japan
Nanopartica Series Instruments (SZ-100)	Horiba	Measurement accuracy; Particle size: ISO 13321/22412 compliant; NIST traceable polystyrene latex particle standard: 100 nm measurement accuracy = +/-2%; Measurement time; Approx. 2 min in general for particle size analysis.	Japan
XRD	Philips X'Pert Modular Powder Diffractometer	This machine operates using a Copper Line Focus X-ray tube with Nickel kβ absorber (0.02 mm; Kβ = 1.392250 Å) producing Kα radiation (Kα1 = 1.540598 Å, Kα2 = 1.544426 Å, Kα ratio 0.5, Kαav = 1.541874 Å); Scan range of 0.75°–143° 2θ	Netherlands
Raman	Horiba LabRAM HR Evolution Micro-Raman Spectrometer	Equipped with a 473 nm diode laser source in the wavenumber range of 100–1000 cm <sup>-1</sup>	Japan
SEM	JEOL 'JSM-7610F'	Resolution (15 kV 0.8 nm, 1 kV 1.0 nm)	Japan

274 nm. The purity of the ZnO NPs confirmed by the absence of other absorption peaks in the spectrum. Fig. 6 and Table 3 show the energy of the band gap is an important factor in photocatalytic activity because the energy of the incident light must be greater than or equal to the energy of the band gap is the criterion for the selection of the photocatalyst [53]. The minimum wavelength required to promote the electron depends on the band gap energy ( $E_g$ ) of the photocatalyst, and the  $E_g$  is calculated using Eq. (1):

$$E_g = \frac{h \cdot c}{\lambda} \quad (1)$$

where  $h$  is Planck's constant ( $6.626 \times 10^{-34}$  Js),  $c$  is the speed of light ( $3 \times 10^8$  m/s), and  $\lambda$  is the cut-off wavelength/

absorption edge in nm. Putting the values ' $h$ ' and ' $c$ ' into Eq. (1) we get the following Eq. (2):

$$E_g = \frac{1240}{\text{outest}} \quad (2)$$

The estimated band gap energy of ZnO was found to be 3.3 eV by putting the value of  $\lambda$  (band edge) = 370 nm from the spectrum.

The characterization of particles by X-ray diffraction (XRD) on a powder gives access to a number of important pieces of information, such as phase identification, quantitative analysis of the phase mixture, and refinement of the crystallographic structure, possibly based on structural assumptions. For this purpose, a structural analysis of X-ray diffractograms complemented by the previous study

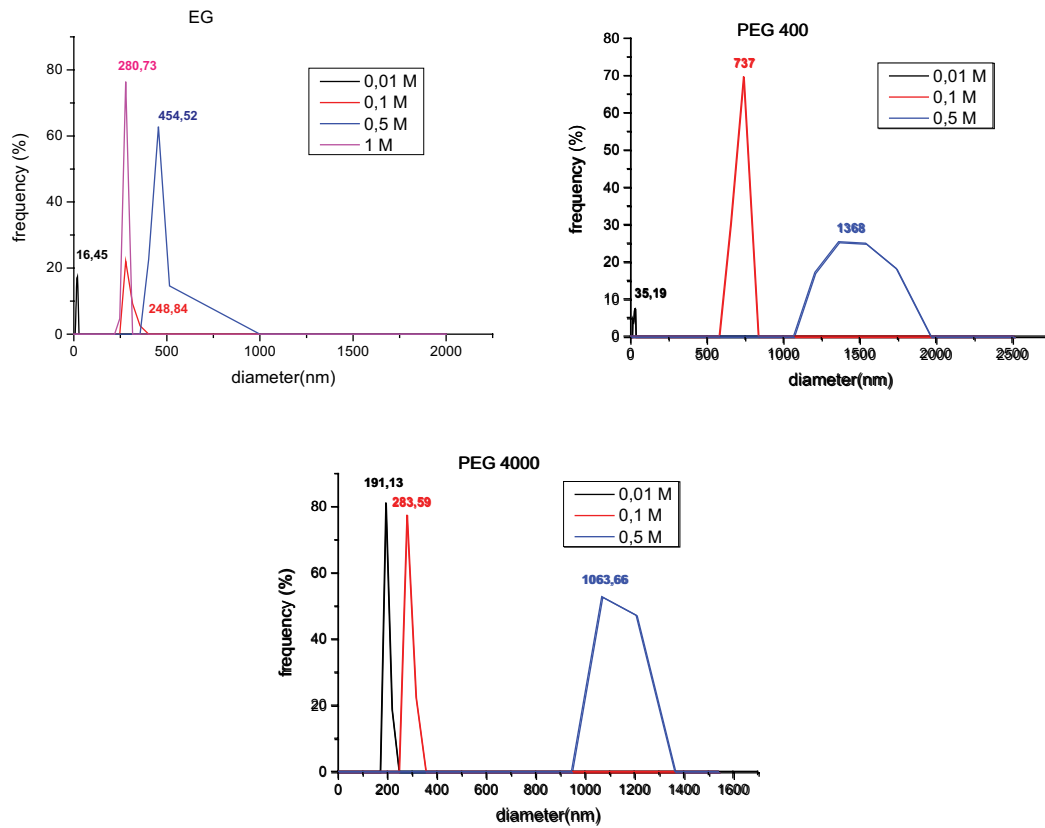


Fig. 3. Size distribution by intensity for EG, PEG400, PEG4000.

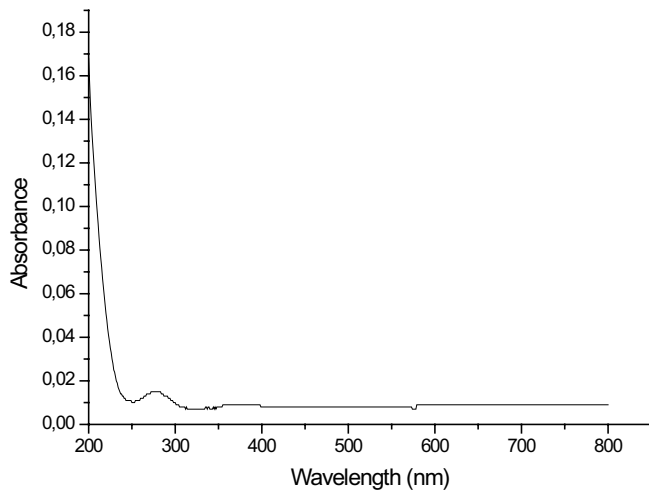


Fig. 4. UV and visible absorption spectra of ZnO.

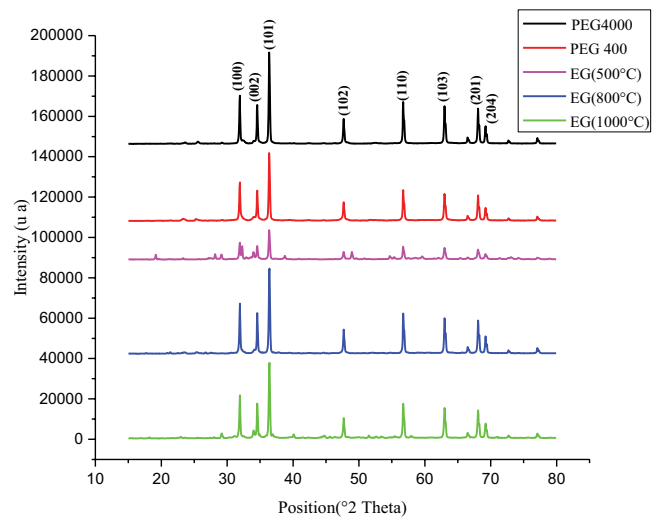


Fig. 5. X-ray diffraction of ZnO.

was systematically performed for all powders to verify the formation of the pure ZnO wurtzite phase for the different preparations and confirm the morphology of the obtained nanoparticles [54].

Fig. 5 indicates the recorded diffractograms. All peaks assigned to the indexed diffraction planes (100), (002), (101), (102), (110), (103), and (201) are in good agreement with the theoretical diffraction peaks of zinc oxide [41]. This result

confirms that the ZnO particles are well crystallized and that the structure is hexagonal of the wurtzite type. Fig. 6 shows the energy-dispersive X-ray (EDS) spectra of ZnO. It can be noted that no impurities are presented in the ZnO-EG and ZnO-PEG nanoparticle samples (400 and 4,000). The peaks corresponding to Zn and O are observed in the EDS spectrum at their normal energy, and the results indicate the formation of ZnO nanoparticles.

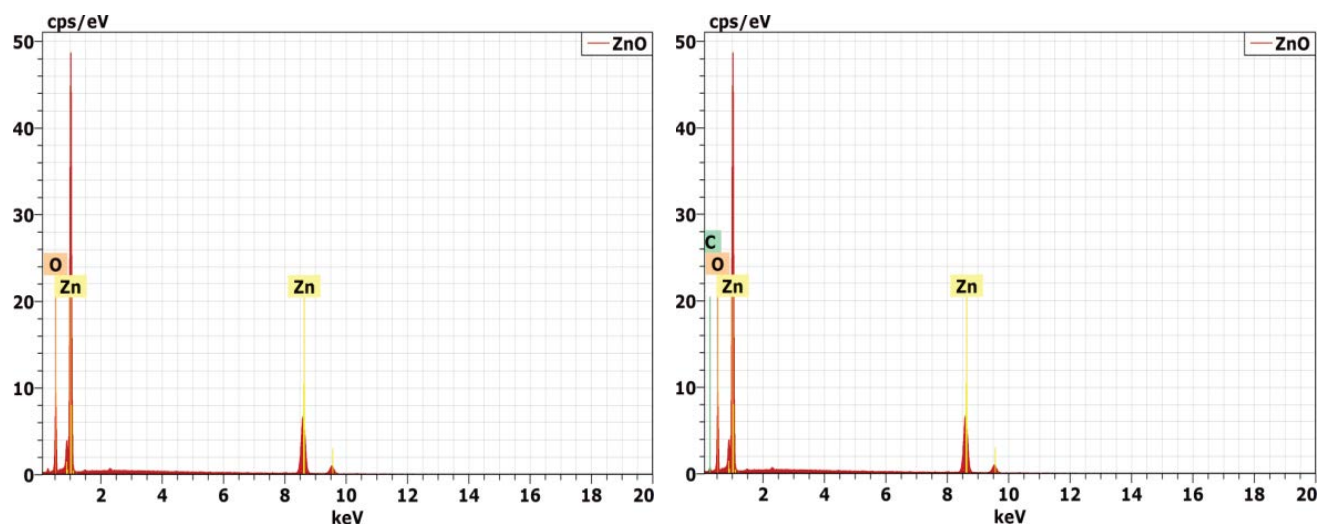


Fig. 6. EDS spectrum of ZnO nanoparticles.

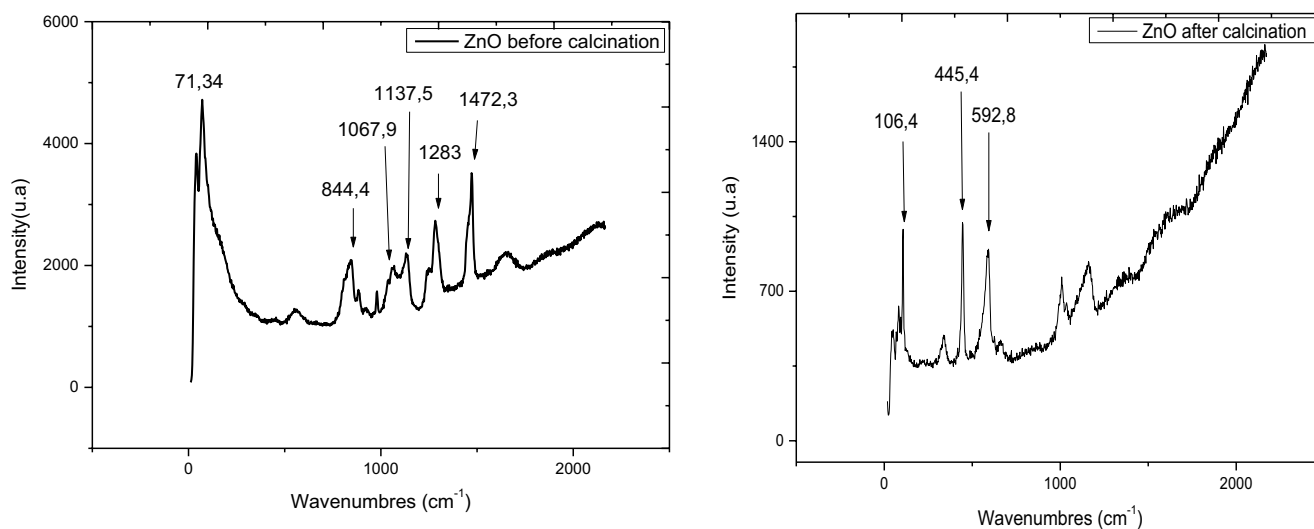


Fig. 7. Raman spectrum of ZnO nanoparticles.

IR spectroscopy provides qualitative information on how the adsorbed PEG molecules are bound to the surface of ZnO nanoparticles. Fig. 8 compares the FTIR spectra of ZnO nanoparticles in the absence and presence of adsorbed PEG at different calcination temperatures. The peaks at 1,649 and 1,216  $\text{cm}^{-1}$  in the spectrum show the formation of PEG on the surface of ZnO nanoparticles. The peak at 3,329  $\text{cm}^{-1}$  suggests the presence of a hydroxyl group. The strong hydroxyl group band in the spectrum of PEG-coated ZnO nanoparticles shifts to a lower wavenumber at 3,329  $\text{cm}^{-1}$ . The peak observed at 437, 440 to 623  $\text{cm}^{-1}$  is due to the elongation vibration of the Zn–O bond. It is the band that characterizes the formation of ZnO [55].

Raman spectroscopy is a non-destructive method to characterize a material's molecular composition and structure. Raman scattering results from light-matter interaction and allows access to molecular and crystalline vibrations. This

technique is complementary to infrared spectroscopy, which also allows the study of a material's vibrational modes. The obtained ZnO nanopowders were also examined by Raman spectroscopy. Fig. 7 shows the results obtained. The peaks of 445.4 and 592.8  $\text{cm}^{-1}$  characterize the formation of ZnO. These results confirm those obtained by IR spectroscopy.

Fig. 9 shows the SEM images of ZnO nanoparticles capped by EG, PEG400, and PEG4000. The results show the transition from a quasi-spherical morphology with EG to rods with PEG400. On the other hand, we obtained nanosheets with PEG4000, which confirms the difference in particle size obtained with the DLS technique, and proves the role of polymer capping on the size and morphology of ZnO nanoparticles. The SEM images also show that the sample with lower molecular weight has a better distribution, as clearly seen in EG's case. However, the larger the alkyl chain, the more aggregated the particles are (case of

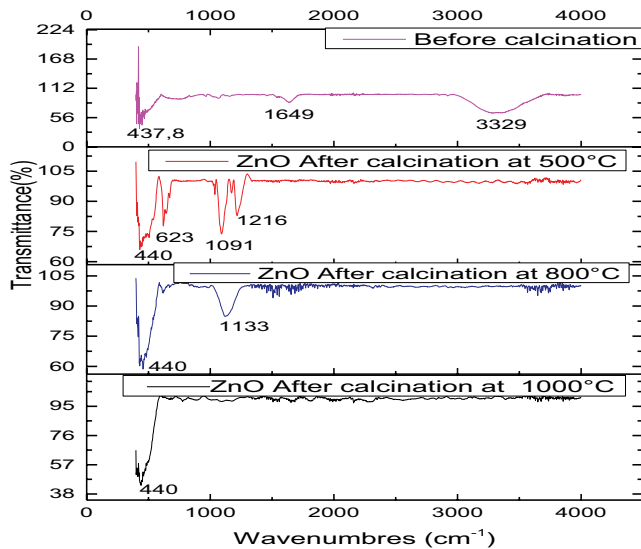


Fig. 8. IR spectrum of the synthesis of ZnO nanoparticles.

PEG4000), which gives an additional explanation for the size variance: zinc ions were better dispersed and more at home in EG than in PEG [56]. This finding may be due to the long chain of PEG, which occupies enough space and prevents the dispersion of zinc ions.

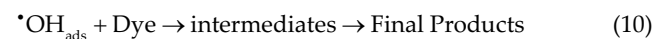
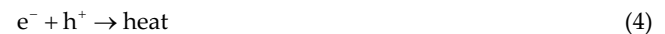
### 3.3. Brunauer–Emmett–Teller analysis of the obtained ZnO nanoparticles

The specific surface area ( $S_{\text{BET}}$ ), pore volume and average diameter (BJH) of obtained ZnO were determined by the adsorption of  $N_2$ . Fig. 8 displays the adsorption–desorption isotherms of  $N_2$ -ZnO. The graph (Fig. 10) displays a type IV isotherm given by the IUPAC classification [57,58]. The isotherm indicates that the pores are filled with gas at extremely low pressure, and then a monolayer starts to form at the knee, while a multilayer is formed when the pressure reaches a medium value [59]. Finally, when the pressure increases, we notice a plateau. The latter indicates that the condensation of gases in the pores of the solid is capillarity, which is known by the phenomenon of hysteresis [60]. The surface area ( $S_{\text{BET}}$ ) of our sample given by the apparatus is about  $134.831 \text{ m}^2/\text{g}$ . The volume of pores equals  $1.230 \text{ cc/g}$ , and the radius of pores  $D_v(r) = 61,937 \text{ \AA}$ . Table 4 summarizes the detailed report calculating the specific surface of ZnO-EG given by the apparatus.

### 3.4. Photolysis, adsorption, and photocatalysis of Brilliant Blue G 250 solutions

Preliminary photolysis and adsorption tests were carried out to demonstrate the effectiveness of combining the two processes (photocatalysis) on the degradation of the Brilliant Blue G 250 dye. The tests are carried out under the following operating conditions: the initial dye concentration equal to  $10 \text{ mg/L}$ , ratio (mass/volume) equal to ( $100 \text{ mg}/100 \text{ mL}$ ), natural pH equal to (6.00), and ambient temperature. Fig. 11a and b confirms the efficiency of the treatment of colored solutions by photocatalysis (ZnO/UV).

The noted removal yields after 1-h treatment are 13.25%, 44.90%, and 87.43% for photolysis, adsorption, and photocatalysis, respectively. The synergistic effect is due to the photo-activation of the synthesized semiconductor with UV irradiations at  $254 \text{ nm}$ , which generates radical species in particular hydroxyl radicals and superoxide ions radicals, according to the following reactions [61,62]:

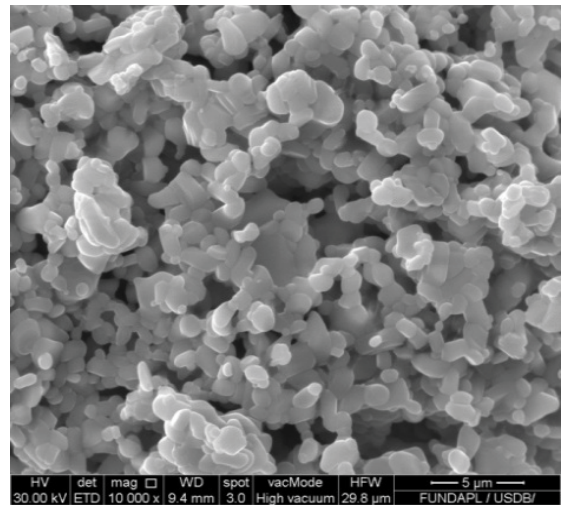
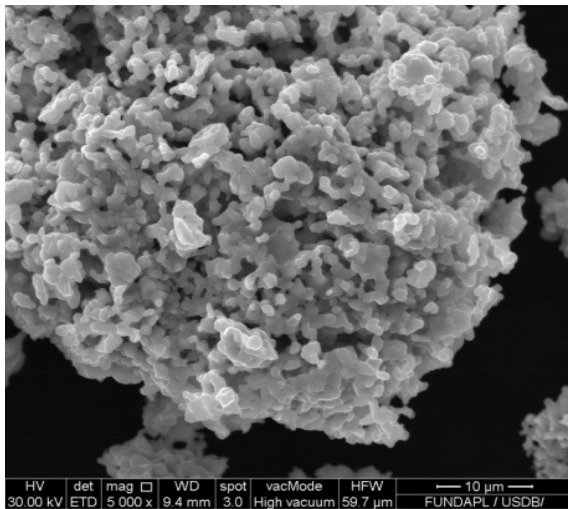


### 3.5. Effect of initial dye concentration

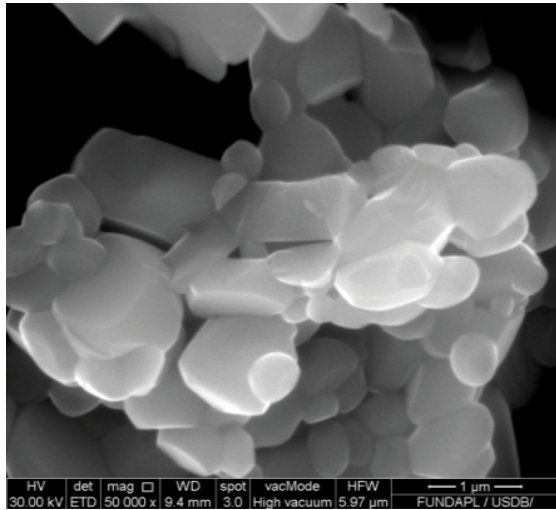
Three different concentrations of dye solutions ( $5$ ,  $10$ , and  $20 \text{ mg/L}$ ) were exposed to the photocatalytic treatment. Fig. 12a indicates that the efficiency after 1h treatment increases with the decrease in the dye concentration. We note 92.78%, 83.37% and 68.13%, respectively, for  $5$ ,  $10$ , and  $20 \text{ mg/L}$ . The increase in the dye content generates an increase in the fraction of adsorbed molecules on the semiconductor's active sites, which prevents the generation of hydroxyl radicals, thus reducing the efficiency of the process [63–67]. Fig. 12b shows the evaluation of the degradation spectra of the  $10 \text{ mg/L}$  solutions of Brilliant Blue G 250 as a function of time. The characteristic peaks of the dye in the UV and Visible zone register a simultaneous decrease during photocatalysis indicating degradation and decolorization.

### 3.6. Effect of photocatalyst mass

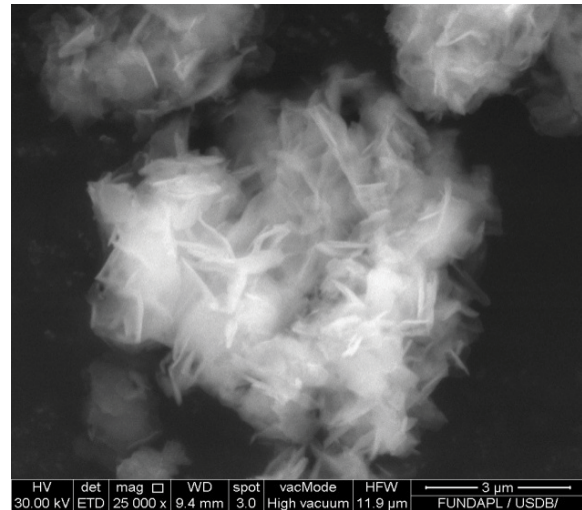
The study of the semiconductor's mass effect on photocatalysis's efficiency was carried out by varying the catalyst content from  $0.01$  to  $1 \text{ g/L}$ . Fig. 13 indicates that after 60 min of treatment the photocatalysis efficiencies increase from 15.05% for  $0.01 \text{ g/L}$ , 52.14% for  $0.1 \text{ g/L}$ , 83.37% for  $0.5 \text{ g/L}$  to 94.32% for  $1 \text{ g/L}$ , while for a mass/volume ratio equal to 2 efficiency decreases. Photocatalysis yield increases by 6.27 for an increasing catalyst factor charge of 100. The improvement in the degradation yields is attributed to the high concentration of different oxidizing species (superoxide radical and hydroxyl radical). The elevated radical's concentrations result from the increased



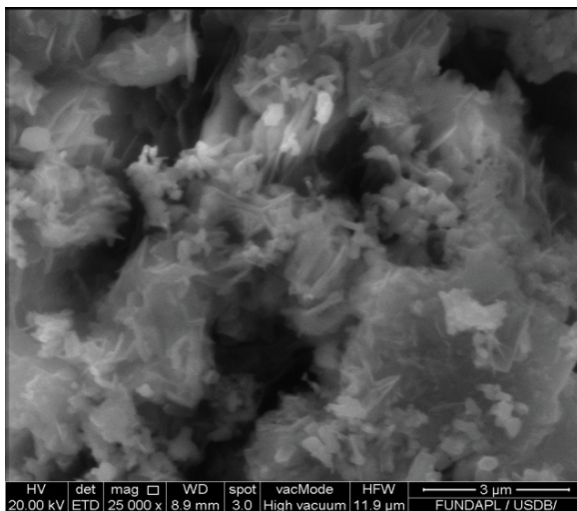
EG



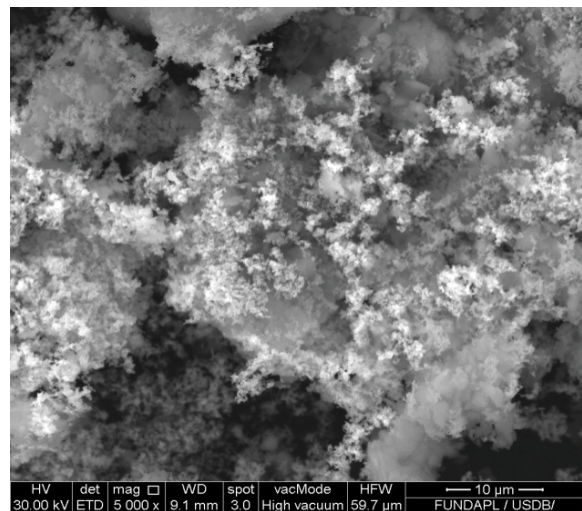
PEG 400



PEG 4000



PEG 4000



PEG 4000

Fig. 9. SEM images of ZnO nanoparticles obtained at 500°C.

number of active sites, which results from increased catalyst concentration [68–74].

### 3.7. Effect of solution's initial pH

The pH plays a crucial role in photocatalytic degradation because the factors controlling the process (the molecule to be degraded, the catalyst, and the oxidizing species) are influenced by the operational values of the pH. The adsorption of Brilliant Blue G 250 dye on ZnO is a function of both the zero-point charge of the catalyst, which is a function of pH and the ionic form of the dye, which is a function of the pKa value. In addition to the medium's predominant form of the oxidizing radical species. The experiments showing the effect of pH were carried out at three different values (4, 9, and 12) for 0.5 mg/L of ZnO and 10 mg/L of Brilliant Blue G 250.

The results illustrated in Fig. 14 show that the highest yield of photocatalytic degradation is recorded at pH 12 for a value equal to 95.67% after 5 min of treatment compared to the yields obtained for pH 04 and pH =  $pH_{PZC} = 09$  for the respective values of 37.55% and 30.53%. NPs of

ZnO are positively charged at pH below their  $pH_{PZC} = 09$  and negatively charged at pH above 9 [75,76]. At the same time, Brilliant Blue G 250 molecules take a positive and negative charge due to both sulfonic and nitrogen groups, which is valid for pH values not exceeding 12 [77]. These two factors can cause an electrostatic interaction between Brilliant Blue G 250 molecules and the catalyst. Also, the results of the photocatalytic oxidation correspond to those obtained during the adsorption of Brilliant Blue G 250 on the semiconductor at the same pH values. These results indicate that the dye's photodegradation occurs at the catalyst's surface. High pH values result in high  $\cdot OH$  concentrations which will also react with the holes ( $h^+$ ) to generate more hydroxyl radicals [62,67,73].

### 3.8. Catalyst recyclability

Another intriguing facet of this protocol is the catalyst's ease of recycling and regeneration. After the catalytic cycle, the catalyst was separated from the solution, washed with methanol in an ultrasonic bath and dried under a vacuum to remove impurities and ensure the purity of the recovered catalyst. The recovered catalyst was then used to test the catalytic efficiency. The results of the recyclability

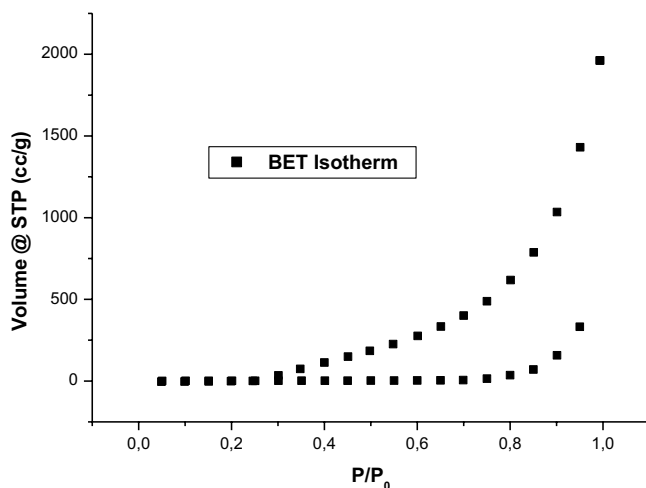


Fig. 10. Nitrogen adsorption–desorption isotherms of ZnO-EG precursor and ZnO-EG nanoparticles.

Table 2

Average diameter for EG, PEG400 and PEG4000 at different concentrations

Synthesis solvent	Concentration	Average diameter (nm)
Ethylene glycol	$C_1 = 0.01M$	16.45
Ethylene glycol	$C_2 = 0.1 M$	280.73
Ethylene glycol	$C_3 = 0.5 M$	454.52
Polyethylene glycol PEG400	$C_1 = 0.01 M$	35.19
Polyethylene glycol PEG400	$C_2 = 0.1 M$	737
Polyethylene glycol PEG400	$C_3 = 0.5 M$	1,368
Polyethylene glycol PEG4000	$C_1 = 0.01 M$	191.13
Polyethylene glycol PEG4000	$C_2 = 0.1 M$	283.59
Polyethylene glycol PEG4000	$C_3 = 0.5 M$	1,063.66

Table 3

EDS analysis

Spectrum: ZnO Sample 1						
Element	Series	Net	unn. (wt.%)	C norm. (wt.%)	C Atom. C Error (at.%)	(3 Sigma) (wt.%)
Zinc	K-series	39,820	57.72	75.81	43.40	4.84
Oxygen	K-series	16,157	18.42	24.19	56.60	7.34
Total:			76.15	100.00	100.00	
Spectrum: ZnO Sample 2						
Zinc	K-series	39,819	54.93	70.45	35.45	4.61
Oxygen	K-series	16,215	18.73	24.02	49.40	7.46
Carbon	K-series	1,070	4.31	5.53	15.15	2.95
Total:			77.97	100.00	100.00	

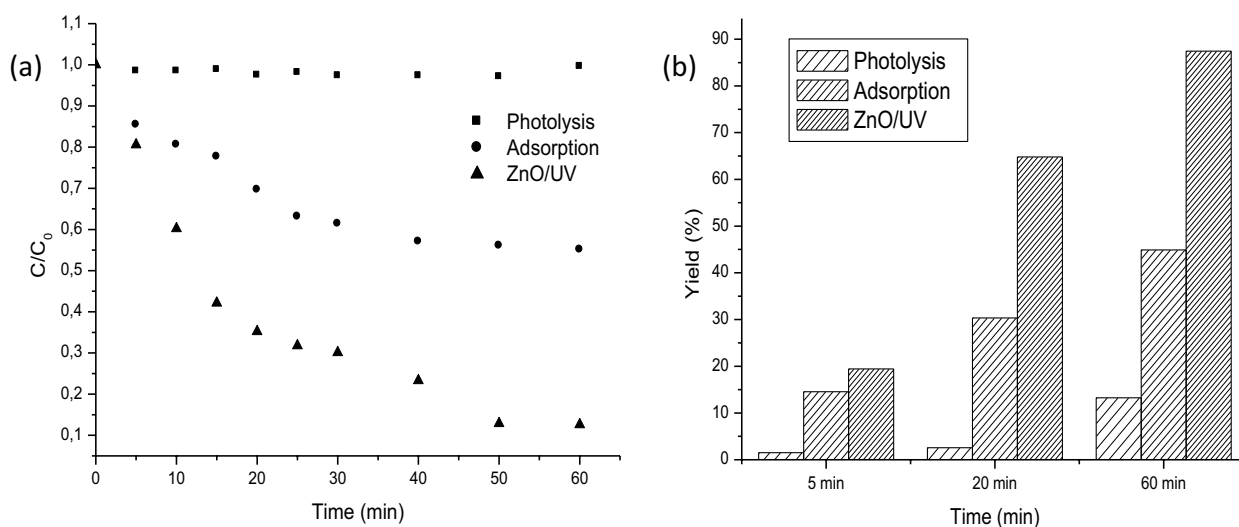


Fig. 11. Photolysis, adsorption, and photocatalysis of BBG solution ( $[BBG]_0 = 10 \text{ mg/L}$ ,  $T = 25^\circ\text{C} \pm 2$ , natural pH = 6.00, agitation rate = 400 tours/min, ZnO mass = 100 mg, and operational volume = 100 mL).

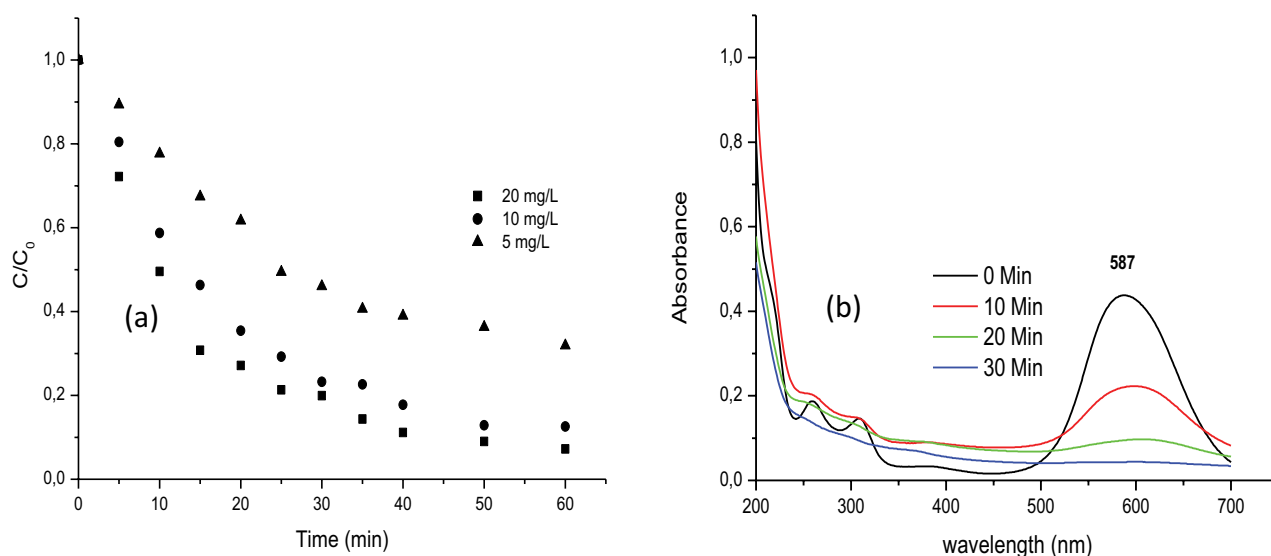


Fig. 12. (a) Effect of initial dye concentration, (b) 10 mg/L Brilliant Blue G 250 degradation spectrum evolution over time ( $[BBG]_0 = 5, 10$  and  $20 \text{ mg/L}$ ,  $T = 25^\circ\text{C} \pm 2$ , natural pH = 6.00, agitation rate = 400 tours/min, ZnO mass = 100 mg, and operational volume = 100 mL).

test are shown in Fig. 15. The ZnO-NPs catalyst shows excellent activity even after three cycles [78].

### 3.9. Comparative study between ZnO and TiO<sub>2</sub> P25

Titanium oxide is the photocatalyst that has been the most studied globally. It can achieve very high yields in photocatalytic degradation reactions of organic compounds. TiO<sub>2</sub> can be crystallized into three different polymorphs: anatase (quadratic), rutile (tetragonal) and metastable brookite (orthorhombic). The photoactivity of anatase is higher than that of rutile. Anatase TiO<sub>2</sub> is a stable polymorph in the low-temperature range but reconverts to rutile at temperatures above 500°C–600°C. TiO<sub>2</sub> absorbs

at wavelengths below 387 and 413 nm for the anatase and rutile forms, respectively. TiO<sub>2</sub>-P25 Degussa is the most widely used titanium oxide in most applications of photocatalytic degradation reactions.

The proportion between the two phases is 80% anatase – 20% rutile. Although TiO<sub>2</sub> in anatase form has been used for many environmental applications, ZnO (gap = 3.2 eV) is also of great interest. The dye decolorization efficiency of ZnO is significantly higher than that of TiO<sub>2</sub>. Some authors have also reported this better photocatalytic efficiency. To confirm this result, a test was carried out between the synthesized ZnO and TiO<sub>2</sub>-P25 (Fig. 16). It can be noticed that from the two curves that the yields after 10, 30 and 60 min of treatment are equal to 11.65%, 57% and 70%, respectively,

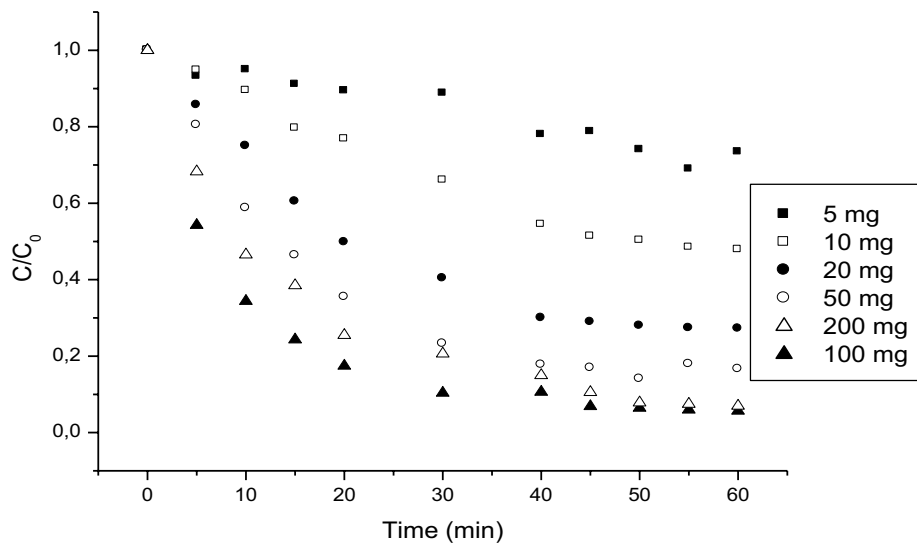


Fig. 13. Effect of catalyst mass ( $[BBG]_0 = 10 \text{ mg/L}$ ,  $T = 25^\circ\text{C} \pm 2$ , natural pH = 6.00, agitation rate = 400 tours/min, and operational volume = 100 mL).

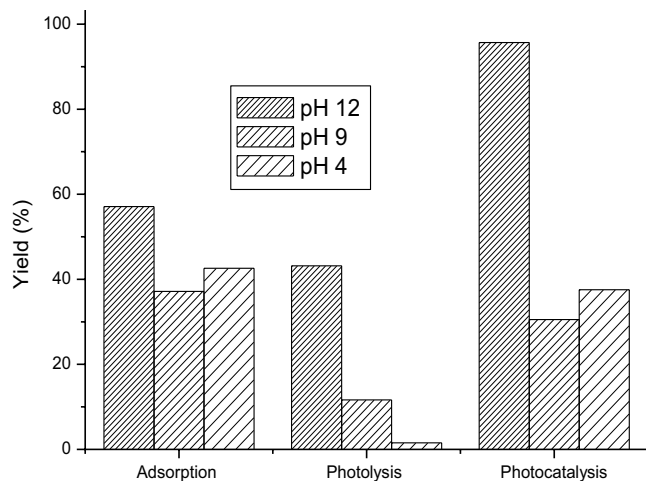


Fig. 14. Effect of the initial pH of solutions ( $[BBG]_0 = 10 \text{ mg/L}$ ,  $T = 25^\circ\text{C} \pm 2$ , agitation rate = 400 tours/min, ZnO mass = 100 mg, and operational volume = 100 mL).

for  $\text{TiO}_2$  compared to those obtained for the synthesized Zn namely 40%, 70% and 87.42%. Such results have been reported by (Qin et al. [79] and Ahmad et al. [80]).

### 3.10. Kinetics model

The pseudo-first-order kinetics was adopted in this study to evaluate the photocatalytic performance of the synthesized ZnO semiconductor during the degradation of Brilliant Blue G 250 under UV irradiation (254 nm). Indeed, the Langmuir–Hinshelwood model describes the proportional relationship between the surface coverage of the support and the dye removal rate:

$$\ln \frac{C_t}{C_0} = -k_{app} t \quad (11)$$

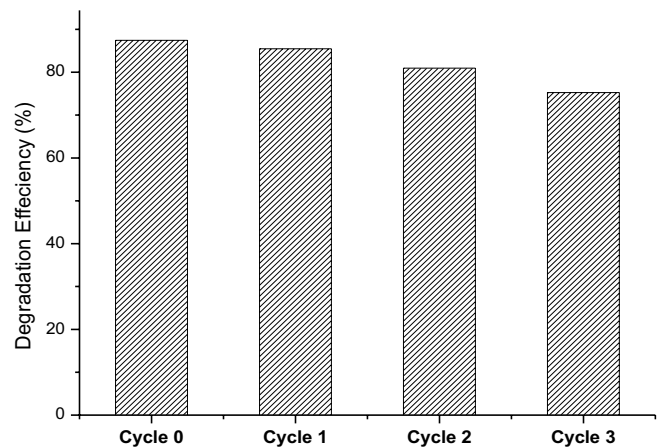


Fig. 15. ZnO-NPs recyclability ( $[BBG]_0 = 10 \text{ mg/L}$ ,  $T = 25^\circ\text{C} \pm 2$ , natural pH, agitation rate = 400 tours/min, ZnO mass = 100 mg, and operational volume = 100 mL).

where  $k_{app}$  ( $\text{min}^{-1}$ ) is the constant of a pseudo-first-order kinetic,  $t$  (min) is the reaction time,  $C_0$  (mg/L) and  $C_t$  (mg/L) are the Brilliant Blue G 250 solution concentrations after the adsorption equilibrium. Fig. 16 represents the linear regression of the equation [Eq. (10)].

As shown in Fig. 17, a pseudo-first-order kinetic represents the kinetics of the photocatalytic degradation of the dye for the three initial concentrations (5, 10, and 20 mg/L) with an adjusted  $R$ -squared of 0.95 [70,74,77,82].

### 3.11. Identification of oxidizing species

Several oxidizing species use their oxidative power to mineralize complex organic molecules during photocatalytic degradation. For this purpose, several trapping molecules are used to identify oxidizing species, including  $t$ -butanol, ascorbic acid and azide for identifying hydroxyl

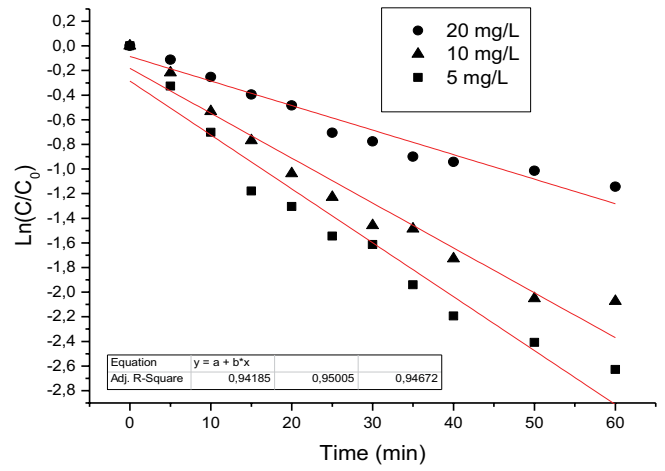
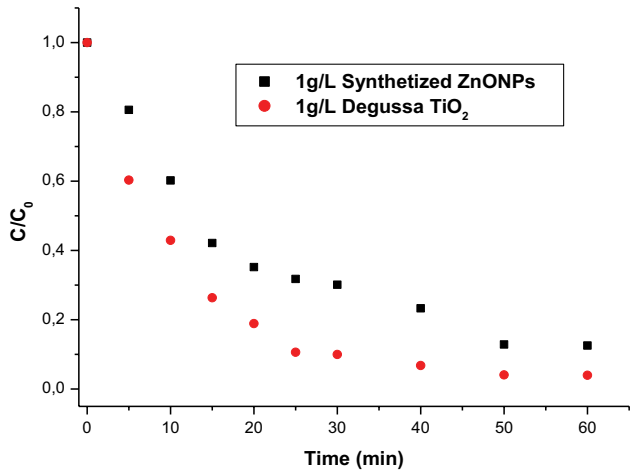


Fig. 16. Photocatalysis kinetics using ZnO and TiO<sub>2</sub> ([BBG]<sub>0</sub> = 10 mg/L, T = 25°C ± 2, natural pH, agitation rate = 400 tours/min, TiO<sub>2</sub> mass = 100 mg, ZnO mass = 100 mg, and operational volume = 100 mL).

Fig. 17. Kinetics of BBG degradation by UV/ZnO-NPs for different initial dye concentrations. ([BBG]<sub>0</sub> = 5, 10 and 20 mg/L, T = 25°C ± 2, natural pH = 6.00, agitation rate = 400 tours/min, ZnO mass = 100 mg, and operational volume = 100 mL).

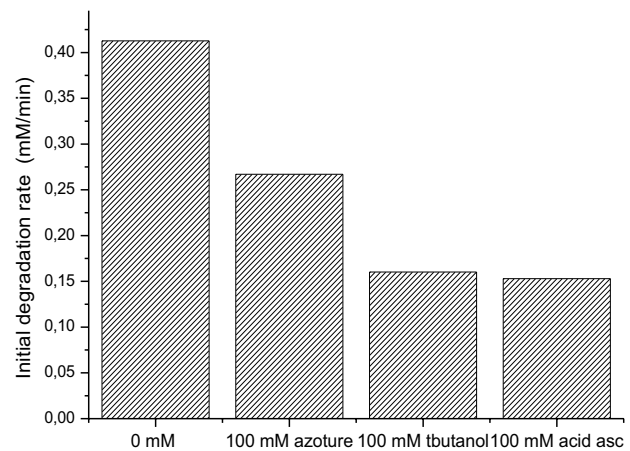
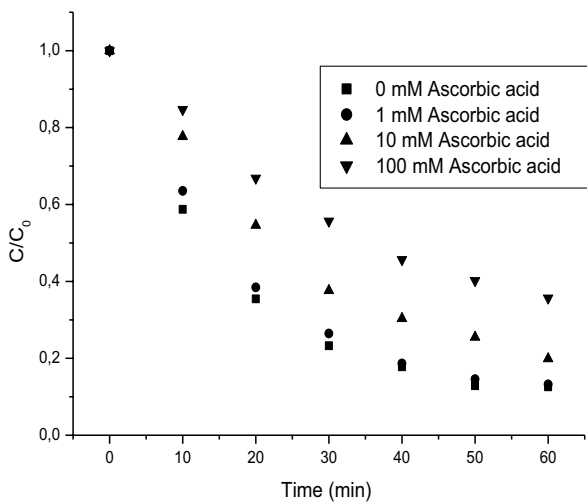
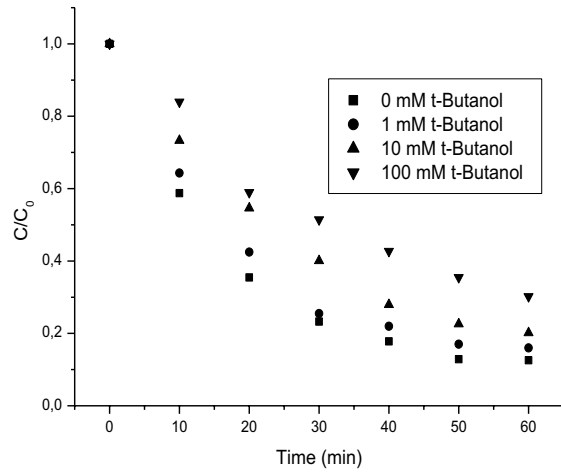
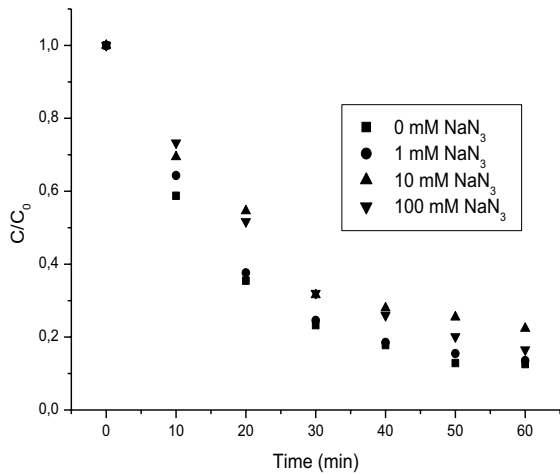


Fig. 18. Scavengers' effect on photocatalytic degradation of Brilliant Blue G 250 ([BBG]<sub>0</sub> = 10 mg/L, T = 25°C ± 2, natural pH, agitation rate = 400 tours/min, ZnO mass = 100 mg, and operational volume = 100 mL).

radicals, superoxide ions and singlet oxygen. The trapping molecules were used at different doses (1, 10 and 100 mM) for a 10 mg/L solution of Brilliant Blue G 250 and 50 mg of synthesized ZnO under UV irradiation (254 nm). Fig. 18 represents the results obtained.

The results indicate that the addition of ascorbic acid, as well as *t*-butanol, has an inhibitory effect on the initial rate of Brilliant Blue G 250 dye degradation calculated after the first 10 min. In contrast, azide has a lesser effect on photodegradation in the following order: Asc (0.15 mM/min), *t*-butanol (0.16 mM/min), azoture (0.27 mM/min) and no Scavengers (0.41 mM/min). This indicates that hydroxyl radicals and superoxide ions are more important than the action of singlet oxygen. Such results are similar to the studies of Kiwaan et al. [82] in the photocatalytic degradation

of Acid Red 57 using synthesized ZnO nanowires, Chen et al. [19] in preparation of ZnO photocatalyst for the efficient and rapid photocatalytic degradation of azo dyes, in addition of Verma et al. [83–85] results' in studies on growth of Au cube-ZnO core-shell nanoparticles for photocatalytic degradation of methylene blue and methyl orange dyes in aqueous media and in presence of different Scavengers [76].

### 3.12. Mineralization of Brilliant Blue G 250

Mineralization of Brilliant Blue G 250 was measured by the total organic carbon (TOC) in an Analytik Jena Analyzer TOC multi-N/C 3100. The percentage of mineralization was estimated using the equation [Eq. (11)]:

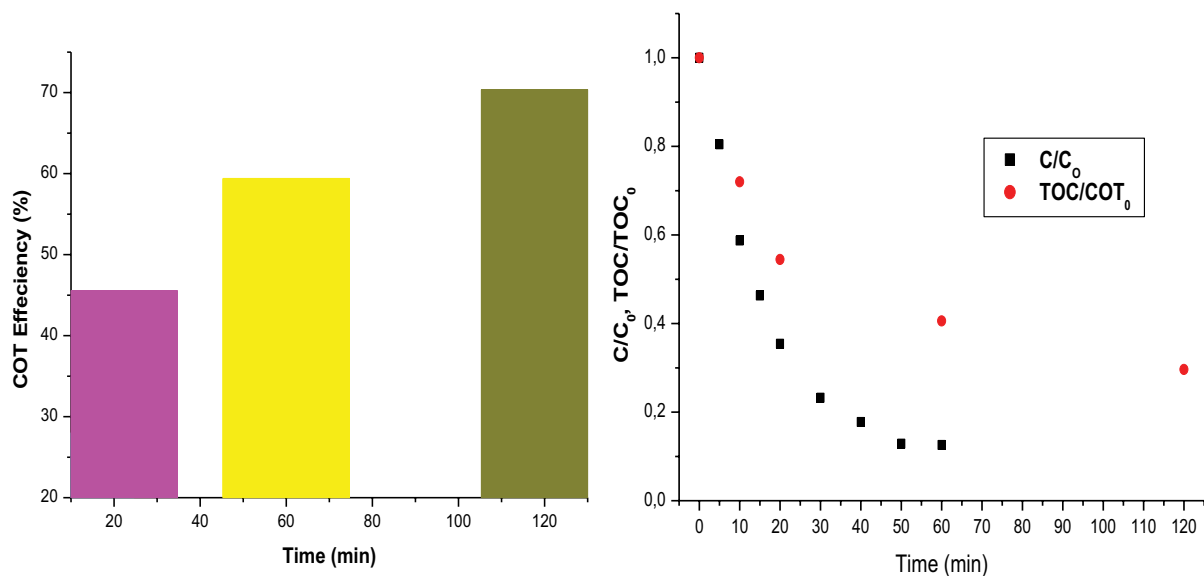


Fig. 19. Mineralization of Brilliant Blue G 250 ( $[BBG]_0 = 10$  mg/L,  $T = 25^\circ\text{C} \pm 2$ , natural pH, agitation rate = 400 tours/min, ZnO mass = 100 mg, and operational volume = 100 mL).

Table 4  
BET analysis of the surface and porosity of the obtained ZnO-EG

Radius Ds (logr) area (Å)	Pore volume (cc/g)	Pore surf (m <sup>2</sup> /g)	dV(r) (cc/Å/g)	dS(r) (m <sup>2</sup> /Å/g)	dV(logr) (cc/g)	dS(logr) (cc/g)
15.3274	0.0000e+00	0.0000e+00	0.0000e+00	0.0000e+00	0.0000e+00	0.0000e+00
17.1183	0.0000e+00	0.0000e+00	0.0000e+00	0.0000e+00	0.0000e+00	0.0000e+00
19.1894	0.0000e+00	0.0000e+00	0.0000e+00	0.0000e+00	0.0000e+00	0.0000e+00
21.6280	0.0000e+00	0.0000e+00	0.0000e+00	0.0000e+00	0.0000e+00	0.0000e+00
24.5589	0.0000e+00	0.0000e+00	0.0000e+00	0.0000e+00	0.0000e+00	0.0000e+00
28.1684	0.0000e+00	0.0000e+00	0.0000e+00	0.0000e+00	0.0000e+00	0.0000e+00
32.7177	1.8383e-03	1.1237e+00	3.6084e-04	2.2058e-01	2.7129e-02	1.6584e+01
38.9136	1.5600e-02	8.1968e+00	1.8859e-03	9.6928e-01	1.6849e-01	8.6594e+01
47.8915	7.1188e-02	3.1411e+01	5.2152e-03	2.1779e+00	5.7272e-01	2.3918e+02
61.9371	1.6374e-01	6.1298e+01	5.3094e-03	1.7145e+00	7.5218e-01	2.4289e+02
86.8573	3.1511e-01	9.6153e+01	4.6708e-03	1.0755e+00	9.2320e-01	2.1258e+02
154.0472	5.4047e-01	1.2541e+02	2.2100e-03	2.8692e-01	7.5437e-01	9.7941e+01
1462.8475	1.2295e+00	1.3483e+02	2.7392e-04	3.7450e-03	6.1369e-01	8.3903e+00

$$\eta = 1 - \frac{\text{TOC}_t}{\text{TOC}_0} \quad (12)$$

Fig. 19 shows the TOC removal efficiency (%) during photocatalytic degradation. The total mineralization after 20 min was found to be 45.54%, 60% after 60 min, and 70% after 120 min. This result indicates that dye degradation was faster than the reduction of TOC, and it represents the resistance of the intermediate product to photocatalytic degradation.

#### 4. Conclusion

In this work, we successfully synthesized ZnO nanoparticles with an average size of 16.45–35.19 nm. We used a simple method by applying ultrasonic waves and modifying the dispersing medium. Various morphologies and sizes were obtained by varying the nature of surfactant used: EG, PEG400, and PEG4000. The higher the number of carbon atoms in the alkyl chain, the larger the particle size. X-ray diffraction analysis of these samples shows the formation of pure phases of ZnO nanoparticles with a wurtzite structure. SEM images show that ZnO nanospheres were synthesized with EG, while nanobats and nanosheets were obtained with PEG400 and PEG4000, respectively. The SEM images also show that the distribution of ZnO nanoparticles improves, and the particles aggregate less than the molecular weight and concentration of PEG decreases. Brunauer–Emmett–Teller (BET) results reveal a type IV isotherm with  $H_3$  hysteresis.

The ZnO-EG synthesized during this work was tested as a semiconductor during the photodegradation of the dye Brilliant Blue G 250. The conducted experiments have shown the effectiveness of the photocatalyst. An efficiency of 87.43% is reached after 60 min of treatment for a mass/liquid ratio equal to 0.5 at natural pH. The efficiency increases with the increase in the mass of the semiconductor to reach 94.32% for 1 g/L. The increase in the dye content decreases the effectiveness of the treatment according to pseudo-first-order kinetics. The degradation is better in alkaline conditions. In addition, the present work indicates that hydroxyl radicals have a major contribution during the photocatalytic process. Also, the abatement of the total organic charge after 120 min equals 70%.

#### Acknowledgment

The support of this investigation by the Ministry of Higher Education and Scientific Research, National Polytechnic School of Constantine – Algeria and the General Directorate of Scientific Research and Technological Development (DGRSDT) is highly acknowledged.

#### Declaration of interests

The authors declare that they have no known competing financial interests or personal relationships that could have appeared to influence the work reported in this paper.

#### References

- [1] D.B. Miklos, C. Remy, M. Jekel, K.G. Linden, J.E. Drewes, U. Hübner, Evaluation of advanced oxidation processes for water and wastewater treatment – a critical review, *Water Res.*, 139 (2018) 118–131.
- [2] H. Zollinger, *Color Chemistry: Synthesis, Properties and Application of Organic Dyes and Pigments*, VCH Publishers, New York, 2004.
- [3] M.A. Brown, S.C. De Vito, Predicting azo dye toxicity, *Crit. Rev. Env. Sci. Technol.*, 23 (1993) 249–324.
- [4] A. Houas, H. Lachheb, M. Ksibi, E. Elaloui, C. Guillard, J.M. Herrmann, Photocatalytic degradation pathway of methylene blue in water, *Appl. Catal., B*, 31 (2001) 145–157.
- [5] E. Sudova, J. Machova, Z. Svobodova, T. Vesely, Negative effects of malachitegreen and possibilities of its replacement in the treatment of fish eggs and fish: a review, *Med. Vet.*, 52 (2007) 527–539.
- [6] Z. Wang, M. Xue, K. Huang, Z. Liu, *Textile Dyeing Wastewater Treatment*, P. Hauser, Ed., *Advances in Treating Textile Effluent*, InTechOpen, China, 2011, pp. 91–116.
- [7] K. Sarayu, S. Sandhya, Current technologies for biological treatment of textile wastewater—a review, *Appl. Biochem. Biotechnol.*, 167 (2012) 645–661.
- [8] K.M.A. Quader, Treatment of textile wastewater with chlorine: an effective method, *Chem. Eng. Res. Bull.*, 14 (2010) 59–63.
- [9] M. Dükkancı, G. Gündüz, Ultrasonic degradation of oxalic acid in aqueous solutions, *Ultrason. Sonochem.*, 13 (2006) 517–522.
- [10] Q. Wang, S. Tian, P. Ning, Degradation mechanism of methylene blue in a heterogeneous Fenton-like reaction catalyzed by ferrocene, *Ind. Eng. Chem. Res.*, 53 (2014) 643–649.
- [11] O. Hamdaoui, M. Chiha, E. Naffrechoux, Ultrasound-assisted removal of malachite green from aqueous solution by dead pine needles, *Ultrason. Sonochem.*, 15 (2008) 799–807.
- [12] S. Merouani, O. Hamdaoui, Y. Rezzgui, M. Guemini, Effects of ultrasound frequency and acoustic amplitude on the size of sonochemically active bubbles—theoretical study, *Ultrason. Sonochem.*, 20 (2013) 815–819.
- [13] Z. Boutamine, O. Hamdaoui, S. Merouani, Probing the radical chemistry and the reaction zone during the sonodegradation of endocrine disruptor 2-phenoxyethanol in water, *Ultrason. Sonochem.*, 41 (2018) 521–526.
- [14] G. Wen, S.J. Wang, J. Ma, T.L. Huang, Z.Q. Liu, L. Zhao, J.L. Xu, Oxidative degradation of organic pollutants in aqueous solution using zero valent copper under aerobic atmosphere condition, *J. Hazard. Mater.*, 275 (2014) 193–199.
- [15] A. Asghar, A. Aziz, A. Raman, W. Mohd, A. Wan, Advanced oxidation processes for *in-situ* production of hydrogen peroxide/hydroxyl radical for textile wastewater treatment: a review, *J. Cleaner Prod.*, 87 (2015) 826–838.
- [16] M.A. Pierrard, P. Kestemont, E. Delaive, M. Dieu, M. Raes, F. Silvestre, Malachite green toxicity assessed on Asian catfish primary cultures of peripheral blood mononuclear cells by a proteomic analysis, *Aquat. Toxicol.*, 114–115 (2012) 142–152.
- [17] I. Boukerche, N. Habbache, N. Alane, S. Djerad, L. Tifouti, Dissolution of cobalt from  $\text{CoO}/\text{Al}_2\text{O}_3$  catalyst with mineral acids, *Ind. Eng. Chem. Res.*, 49 (2010) 6514–6520.
- [18] R. Larba, I. Boukerche, N. Alane, N. Habbache, S. Djerad, L. Tifouti, Citric acid as an alternative lixiviant for zinc oxide dissolution, *Hydrometallurgy*, 134–135 (2013) 117–123.
- [19] D. Chen, X. Jiao, G. Cheng, Hydrothermal synthesis of zinc oxide powders with different morphologies, *Solid State Commun.*, 113 (2000) 363–366.
- [20] S.J. Peaton, D.P. Norton, K. Ip, Y.W. Heo, T. Steiner, Recent progress in processing and properties of ZnO, *Superlattices Microstruct.*, 34 (2003) 3–32.
- [21] J.Q. Hu, X.L. Ma, Z.Y. Xie, N.B. Wong, C.S. Lee, S.T. Lee, Characterization of zinc oxide crystal whiskers grown by thermal evaporation, *Chem. Phys. Lett.*, 344 (2000) 97–100.
- [22] I. Boukerche, S. Djerad, L. Benmansour, L. Tifouti, K. Saleh, Degradability of aluminum in acidic and alkaline solutions, *Corros. Sci.*, 78 (2014) 343–352.

- [23] W.J. Li, E.W. Shi, W.Z. Zhong, Z. Yin, Growth mechanism and growth habit of oxide crystals, *J. Cryst. Growth*, 203 (1999) 186–196.
- [24] C. Lu, C. Yeh, Influence of hydrothermal conditions on the morphology and particle size of zinc oxide powder, *Ceram. Int.*, 26 (2000) 351–357.
- [25] B.G. Wang, E.W. Shi, W.Z. Zhong, Twinning morphologies and mechanisms of ZnO crystallites under hydrothermal conditions, *Cryst. Res. Technol.*, 33 (1998) 937–941.
- [26] L. Chetibi, A. Achour, J. Peszke, D. Hamana, S. Achour, Hydroxyapatite growth on multiwall carbon nanotubes grown on titanium fibers from a titanium sheet, *J. Mater. Sci.*, 49 (2014) 621–632.
- [27] O. Hamdaoui, E. Naffrechoux, Sonochemical and photosonochemical degradation of 4-chlorophenol in aqueous media, *Ultrason. Sonochem.*, 15 (2008) 981–987.
- [28] M. Chiha, O. Hamdaoui, F. Ahmed Chekkat, C. Pétrier, Study on ultrasonically assisted emulsification and recovery of copper(II) from wastewater using an emulsion liquid membrane process, *Ultrason. Sonochem.*, 17 (2010) 318–325.
- [29] Q.P. Isariebel, J.L. Carine, J.H. Ulises-Javier, W. Anne-Marie, D. Henri, Sonolysis of levodopa and paracetamol in aqueous solutions, *Ultrason. Sonochem.*, 16 (2009) 610–616.
- [30] T. Hongo, M. Moriura, Y. Hatada, H. Abiko, Simultaneous methylene blue adsorption and pH neutralization of contaminated water by rice husk ash, *ACS Omega*, 6 (2021) 21604–21612.
- [31] S. Zinatloo-Ajabshir, M. Salavati-Niasari, Preparation of magnetically retrievable  $\text{CoFe}_2\text{O}_4/\text{SiO}_2/\text{Dy}_2\text{Ce}_2\text{O}_7$  nanocomposites as novel photocatalyst for highly efficient degradation of organic contaminants, *Composites, Part B*, 174 (2019) 106930.
- [32] S. Zinatloo-Ajabshir, S. Mortazavi-Derazkola, M. Salavati-Niasari,  $\text{Nd}_2\text{O}_3\text{-SiO}_2$  nanocomposites: a simple sonochemical preparation, characterization and photocatalytic activity, *Ultrason. Sonochem.*, 42 (2018) 171–182.
- [33] F. Davar, M. Salavati-Niasari, Z. Fereshteh, Synthesis and characterization of  $\text{SnO}_2$  nanoparticles by thermal decomposition of new inorganic precursor, *J. Alloys Compd.*, 496 (2010) 638–643.
- [34] M. Hassanpour, H. Safardoust-Hojaghan, M. Salavati-Niasari, Degradation of methylene blue and Rhodamine B as water pollutants via green synthesized  $\text{Co}_3\text{O}_4/\text{ZnO}$  nanocomposite, *J. Mol. Liq.*, 229 (2017) 293–299.
- [35] M. Ghiyasiyan-Arani, M. Salavati-Niasari, Enhanced photodegradation of dye in wastewater using iron vanadate nanocomposite; ultrasound-assisted preparation and characterization, *Ultrason. Sonochem.*, 39 (2017) 494–503.
- [36] M. Panahi-Kalamuei, S. Alizadeh, M. Mousavi-Kamazani, M. Salavati-Niasari, Synthesis and characterization of  $\text{CeO}_2$  nanoparticles via hydrothermal route, *J. Ind. Eng. Chem.*, 21 (2015) 1301–1305.
- [37] T. Gholami, M. Salavati-Niasari, S. Varshoy, Electrochemical hydrogen storage capacity and optical properties of  $\text{NiAl}_2\text{O}_4/\text{NiO}$  nanocomposite synthesized by green method, *Int. J. Hydrogen Energy*, 42 (2017) 5235–5245.
- [38] A. Francony, C. Pétrier, Sonochemical degradation of carbon tetrachloride in aqueous solution at two frequencies: 20 kHz and 500 kHz, *Ultrason. Sonochem.*, 3 (1996) S77–S82.
- [39] R. Monsef, M. Ghiyasiyan-Arani, M. Salavati-Niasari, Application of ultrasound-aided method for the synthesis of  $\text{NdVO}_4$  nano-photocatalyst and investigation of eliminate dye in contaminant water, *Ultrason. Sonochem.*, 42 (2018) 201–211.
- [40] K. Krishnamoorthy, S.J. Kim, Growth, characterization and electrochemical properties of hierarchical CuO nanostructures for super capacitor applications, *Mater. Res. Bull.*, 48 (2013) 3136–3139.
- [41] H.K. Farag, R.M.M. Aboelenin, N.A. Fathy, Photodegradation of methyl orange dye by ZnO loaded onto carbon xerogels composites, *Asia-Pac. J. Chem. Eng.*, 12 (2017) 4–12.
- [42] S.M. El-Khouly, G.M. Mohamed, N.A. Fathy, G.A. Fagal, Effect of nanosized  $\text{CeO}_2$  or ZnO loading on adsorption and catalytic properties of activated carbon, *Adsorpt. Sci. Technol.*, 35 (2017) 774–788.
- [43] N.N. Fathima, R. Aravindhan, J.R. Rao, B.U. Nair, Dye house wastewater treatment through advanced oxidation process using Cu-exchanged Y zeolite: a heterogeneous catalytic approach, *Chemosphere*, 70 (2008) 1146–1151.
- [44] Z. Sharifalhosseini, M.H. Entezari, R. Jalal, Direct and indirect sonication affect differently the microstructure and the morphology of ZnO nanoparticles: optical behavior and its antibacterial activity, *Ultrason. Sonochem.*, 27 (2015) 466–473.
- [45] J. Zhang, L. Sun, H. Pan, C. Liao, C. Yan, ZnO nanowires fabricated by a convenient route, *New J. Chem.*, 26 (2002) 33–34.
- [46] S.M. Haile, D.W. Johnson, G.H. Wiseman, H.K. Bowen, Aqueous precipitation of spherical zinc oxide powders for varistor applications, *J. Am. Ceram. Soc.*, 72 (1989) 2004–2008.
- [47] K. Sue, K. Kimura, M. Yamamoto, K. Arai, Rapid hydrothermal synthesis of ZnO nanorods without organics, *Mater. Lett.*, 58 (2004) 3350–3352.
- [48] E. Ohshima, H. Ogino, I. Niikura, K. Maeda, M. Sato, M. Ito, T. Fukuda, Growth of the 2-in-size bulk ZnO single crystals by the hydrothermal method, *J. Cryst. Growth*, 260 (2004) 166–170.
- [49] M. Yoshimura, Importance of soft solution processing for advanced inorganic materials, *J. Mater. Res.*, 13 (1998) 796–802.
- [50] S. Koda, T. Kimura, T. Kondo, H. Mitome, A standard method to calibrate sonochemical efficiency of an individual reaction system, *Ultrason. Sonochem.*, 10 (2003) 149–156.
- [51] C. Guoliang, N. Xiaodong, N. Timothée, Lattice parameter dependence on long-range ordered degree during order-disorder transformation, *Intermetallics*, 12 (2004) 733–739.
- [52] V. Leena Bora, K.R. Mewada, Photocatalytic decolouration, degradation and disinfection capability of  $\text{Ag}_2\text{CO}_3/\text{ZnO}$  in natural sunlight, *J. Indian Chem. Soc.*, 99 (2022) 100311, doi: 10.1016/j.jics.2021.100311.
- [53] A. Bhirud, S. Sathaye, R. Waichal, C.J. Park, B. Kale, *In-situ* preparation of N-ZnO/graphene nanocomposites: excellent candidate as a photocatalyst for enhanced solar hydrogen generation and high-performance supercapacitor electrode, *J. Mater. Chem.*, 3 (2015) 17050–17063.
- [54] A.N. Kadam, R.S. Dhabbe, M.R. Kokate, K.M. Garadkar, Room temperature synthesis of CdS nanoflakes for photocatalytic properties, *J. Mater. Sci. - Mater. Electron.*, 25 (2014) 1887–1892.
- [55] W. Changle, Q. Xueliang, C. Jianguo, W. Hongshui, T. Fatang, L. Shitao, A novel chemical route to prepare Zn nanoparticles, *Mater. Lett.*, 60 (2006) 1828–1832.
- [56] S.K.N. Ayudhya, P. Tonto, O. Mekasuwandumrong, V. Pavarajarn, P. Praserttham, Solvothermal synthesis of ZnO with various aspect ratios using organic solvents, *Cryst. Growth Des.*, 6 (2006) 2446–2450.
- [57] M.A. Ismail, K.K. Taha, A. Modwi, L. Khezami, ZnO nanoparticles: surface and X-ray profile analysis, *J. Ovonic Res.*, 14 (2018) 381–393.
- [58] T. Pandiyarajan, B. Karthikeyan, Cr doping induced structural, phonon and excitonic properties of ZnO nanoparticles, *J. Nanopart. Res.*, 14 (2012) 647, doi: 10.1007/s11051-011-0647-x.
- [59] S. Kuśnieruk, J. Wojnarowicz, A. Chodara, T. Chudoba, S. Gierlotka, W. Lojkowski, Influence of hydrothermal synthesis parameters on the properties of hydroxyapatite nanoparticles, *Beilstein J. Nanotechnol.*, 7 (2016) 1586–1601.
- [60] V. Bolis, B. Fubini, E. Giamello, Effect of form on the surface reactivity of differently prepared zinc oxides, *J. Chem. Soc., Faraday Trans. 1 F*, 85 (1989) 855–867.
- [61] M.A. Behnajady, N. Modirshahla, R. Hamzavi, Kinetic study on photocatalytic degradation of CI Acid Yellow 23 by ZnO photocatalyst, *J. Hazard. Mater.*, 33 (2006) 226–232.
- [62] B.S. Bukallah, M.A. Rauf, S. Ashraf, Photocatalytic decoloration of Coomassie Brilliant Blue with titanium oxide, *Dyes Pigm.*, 72 (2007) 353–356.
- [63] C.H. Wu, Comparison of azo dye degradation efficiency using UV/single semiconductor and UV/coupled semiconductor systems, *Chemosphere*, 57 (2004) 601–608.
- [64] M. Qamar, M. Saquib, M. Muneer, Photocatalytic degradation of two selected dye derivatives, chromotrope 2B and amido

- black 10B, in aqueous suspensions of titanium dioxide, *Dyes Pigm.*, 65 (2005) 1–9.
- [65] N. Daneshvar, M. Rabbani, N. Modirshahla, M.A. Behnajady, Kinetic modeling of photocatalytic degradation of Acid Red 27 in UV/TiO<sub>2</sub> process, *J. Photochem. Photobiol.*, 168 (2004) 39–45.
- [66] R. Kumar, G. Kumar, A. Umar, ZnO nano-mushrooms for photocatalytic degradation of methyl orange, *Mater. Lett.*, 97 (2013) 100–103.
- [67] M. Bagheri, A.R. Mahjoub, B. Mehri, Enhanced photocatalytic degradation of Congo red by solvothermally synthesized CuInSe<sub>2</sub>-ZnO nanocomposites, *R. Soc. Chem.*, 4 (2014) 21757–21764.
- [68] I.K. Konstantinou, T.A. Albanis, TiO<sub>2</sub>-assisted photocatalytic degradation of azo dyes in aqueous solution: kinetic and mechanistic investigations: a review, *Appl. Catal.*, 49 (2004) 1–14.
- [69] M. Pera-Titus, V.G. Molina, M.A. Banos, J. Gimenez, S. Esplugas, Optimization of photocatalytic degradation of phenol using simple photocatalytic reactor, *Appl. Catal.*, 47 (2004) 219–256.
- [70] S. Chakrabarti, B.K. Dutta, Photocatalytic degradation of model textile dyes in wastewater using ZnO as semiconductor catalyst, *J. Hazard. Mater.*, 112 (2004) 269–278.
- [71] I. Kazeminezhad, A. Sadollahkhani, Influence of pH on the photocatalytic activity of ZnO nanoparticles, *J. Mater. Sci.: Mater. Electron.*, 27 (2016) 4206–4215.
- [72] C. Xiaoqing, W. Zhansheng, L. Dandan, G. Zhenzhen, Preparation of ZnO photocatalyst for the efficient and rapid photocatalytic degradation of azo dyes, *Nanoscale Res. Lett.*, 12 (2017) 143, doi: 10.1186/s11671-017-1904-4.
- [73] M.O. Fatehah, H.A. Aziz, S. Stoll, Stability of ZnO nanoparticles in solution. Influence of pH, dissolution, aggregation and disaggregation effects, *J. Colloid Sci. Biotechnol.*, 3 (2014) 75–84.
- [74] M. Malakootiana, A. Nasiria, A.N. Alibeigic, H. Mahdizadehb, M.A. Gharaghanic, Synthesis and stabilization of ZnO nanoparticles on a glass plate to study the removal efficiency of acid red 18 by hybrid advanced oxidation process (ultraviolet/ZnO/ultrasonic), *Desal. Water Treat.*, 170 (2019) 325–336.
- [75] H.J. Chial, H.B. Thompson, A.G. Splittgerber, A spectral study of the charge forms of Coomassie Blue G, *Anal. Biochem.*, 209 (1993) 258–266.
- [76] T. Parvin, N. Keerthiraj, I.A. Ibrahim, S. Phanichphant, K. Byrappa, Photocatalytic degradation of municipal wastewater and Brilliant Blue dye using hydrothermally synthesized surface-modified silver-doped ZnO designer particles, *Int. J. Photoenergy*, 2012 (2012) 670610, 8 pages.
- [77] L.T.T. Nguyen, D. Viet N. Vo, L.T.H. Nguyen, A.T.T. Duong, H.Q. Nguyen, N.M. Chu, D.T.C. Nguyen, T.V. Tran, Synthesis, characterization, and application of ZnFe<sub>2</sub>O<sub>4</sub>@ZnO nanoparticles for photocatalytic degradation of Rhodamine B under visible-light illumination, *Environ. Technol. Innovation*, 25 (2022) 102130, doi: 10.1016/j.eti.2021.102130.
- [78] L. Pan, G.Q. Shen, J.W. Zhang, X.C. Wei, L. Wang, J.J. Zou, X. Zhang, TiO<sub>2</sub>-ZnO composite sphere decorated with ZnO clusters for effective charge, *Ind. Eng. Chem. Res.*, 54 (2015) 7226–7232.
- [79] R. Qin, F. Meng, M.W. Khan, B. Yu, H. Li, Z. Fan, J. Gong, Fabrication and enhanced photocatalytic property of TiO<sub>2</sub>-ZnO composite photocatalysts, *Mater. Lett.*, 240 (2019) 84–87.
- [80] M. Ahmad, W. Rehman, M.M. Khan, M.T. Qureshi, A. Gul, S. Haq, R. Ullah, A. Rab, F. Mena, Phylogenetic fabrication of ZnO and gold decorated ZnO nanoparticles for photocatalytic degradation of Rhodamine B, *J. Environ. Chem. Eng.*, 9 (2021) 104725, doi: 10.1016/j.jece.2020.104725.
- [81] M.A. Behnajady, N. Modirshahla, R. Hamzavi, Kinetic study on photocatalytic degradation of C.I. Acid Yellow 23 by ZnO photocatalyst, *J. Hazard. Mater.*, 133 (2006) 226–232.
- [82] H.A. Kiwaan, T.M. Atwee, E.A. Azab, A.A. El-Bindary, Efficient photocatalytic degradation of Acid Red 57 using synthesized ZnO nanowires, *J. Chin. Chem. Soc.*, 66 (2018) 1–10.
- [83] N. Verma, S. Bhatia, R.K. Bedi, Role of pH on electrical, optical and photocatalytic properties of ZnO based nanoparticles, *J. Mater. Sci.: Mater. Electron.*, 28 (2017) 9788–9797.
- [84] S. Verma, B.T. Rao, J. Jayabalan, S.K. Rai, D.M. Phase, A.K. Srivastava, R. Kaul, Studies on growth of Au cube-ZnO core-shell nanoparticles for photocatalytic degradation of methylene blue and methyl orange dyes in aqueous media and in presence of different Scavengers, *J. Environ. Chem. Eng.*, 7 (2019) 103209, doi: 10.1016/j.jece.2019.103209.
- [85] S. Verma, B.T. Rao, R. Singh, R. Kaul, Photocatalytic degradation kinetics of cationic and anionic dyes using Au-ZnO nanorods: role of pH for selective and simultaneous degradation of binary dye mixtures, *Ceram. Int.*, 47 (2021) 34751–34764.